ARMY RESEARCH LABORATORY

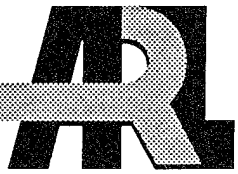

The Terminal Ballistic Performance of Microstructural Oriented Tungsten Heavy Alloy Penetrators

Wendy Leonard
Lee Magness

ARL-TR-881 October 1995

NOTICES

Destroy this report when it is no longer needed. DO NOT return it to the originator.

Additional copies of this report may be obtained from the National Technical Information Service, U.S. Department of Commerce, 5285 Port Royal Road, Springfield, VA 22161.

The findings of this report are not to be construed as an official Department of the Army position, unless so designated by other authorized documents.

The use of trade names or manufacturers' names in this report does not constitute indorsement of any commercial product.

REPORT DOCUMENTATION PAGE

Form Approved
OMB No. 0704-0188

1. AGENCY USE ONLY *(Leave blank)*	2. REPORT DATE	3. REPORT TYPE AND DATES COVERED
	October 1995	Final, October–November 1991

4. TITLE AND SUBTITLE

The Terminal Ballistic Performance of Microstructural Oriented Tungsten Heavy Alloy Penetrators

5. FUNDING NUMBERS

PR: 1L162618AH80

6. AUTHOR(S)

Wendy Leonard and Lee Magness

7. PERFORMING ORGANIZATION NAME(S) AND ADDRESS(ES)

U.S. Army Research Laboratory
ATTN: AMSRL-WT-TC
Aberdeen Proving Ground, MD 21005-5066

8. PERFORMING ORGANIZATION REPORT NUMBER

ARL-TR-881

9. SPONSORING/MONITORING AGENCY NAME(S) AND ADDRESS(ES)

10. SPONSORING/MONITORING AGENCY REPORT NUMBER

11. SUPPLEMENTARY NOTES

12a. DISTRIBUTION/AVAILABILITY STATEMENT

Approved for public release; distribution is unlimited.

12b. DISTRIBUTION CODE

13. ABSTRACT *(Maximum 200 words)*

A study was conducted to investigate the influence of microstructural orientation on tungsten heavy alloy penetrator performance. The penetration performance of model-scale penetrators with a heavily worked microstructure oriented parallel, perpendicular, and at 30°, 45°, and 60° with respect to the penetrator axis were compared in ballistic tests. Residual penetrators were recovered, and the deformation of each microstructural orientation was examined.

14. SUBJECT TERMS

penetration performance, shear localization, microsctructural orientation, deformation

15. NUMBER OF PAGES

46

16. PRICE CODE

17. SECURITY CLASSIFICATION OF REPORT	18. SECURITY CLASSIFICATION OF THIS PAGE	19. SECURITY CLASSIFICATION OF ABSTRACT	20. LIMITATION OF ABSTRACT
UNCLASSIFIED	UNCLASSIFIED	UNCLASSIFIED	UL

INTENTIONALLY LEFT BLANK.

ACKNOWLEDGMENTS

The authors would like to acknowledge the efforts of the Range 110 Director, Eleanor Deal, and the engineering technicians, B. McKay, J. Koontz, M. Clark, V. Torbert, and R. English, for their timely completion of the ballistic firings. Additional acknowledgment is given to V. Torbert for specimen preparation and polishing of the sectioned targets.

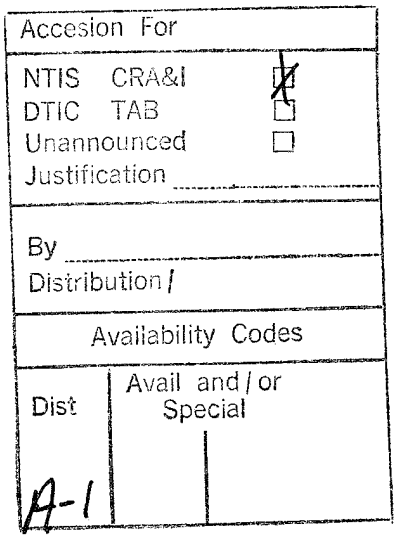

INTENTIONALLY LEFT BLANK.

TABLE OF CONTENTS

INTENTIONALLY LEFT BLANK.

LIST OF FIGURES

LIST OF TABLES

INTENTIONALLY LEFT BLANK.

1. INTRODUCTION

A long, sought-after goal of Department of Defense (DOD) research has been the development of a tungsten heavy alloy (WHA) penetrator material offering terminal ballistic performance equaling or surpassing that of depleted uranium (DU). Several studies (Magness and Farrand 1990; Meyer et al. 1990; Woolsey 1992; Leonard, Magness, and Kapoor 1992), however, have concluded that the conventional engineering properties of strength, ductility, toughness, etc., have little or no influence on the fundamental penetration capabilities of WHAs. Despite significant improvements in the tensile strengths, tensile elongations, and toughnesses of WHAs, in many cases exceeding the properties of DU alloys, the ballistic performance of those alloys did not significantly differ from that of WHAs of conventional processing and properties (Leonard, Magness, and Kapoor 1992), and the shortfall with respect to DU performance remained.

Recent studies (Magness and Farrand 1990) have demonstrated that the flow and failure behavior of penetrator materials, a function of both mechanical and thermal properties, determine the penetration performance of these high-density materials. Under the high-pressure, high-rate loading conditions of the penetration event, thermal softening of the penetrator material (due to the heat generated internally with the deformation) competes with, and eventually overcomes, the strengthening mechanisms of deformation (strain-hardening and strain-rate-hardening). Once the penetrator material softens rather than strengthens with strain, the deformation may quickly localize as adiabatic shear failures or bands. For DU alloy penetrators, the rapid development of this flow and failure behavior leads to a quick discard of penetrator material deformed at the head of the penetrator. This reduces the size of the head that builds up on the projectile (Figure 1) and allows the DU penetrator to efficiently burrow a smaller diameter, but deeper, cavity into armor. Conventional tungsten-nickel-iron alloy penetrator materials do not flow-soften as quickly as DU. Plastic localizations will develop only after the WHA has undergone very large plastic strains, producing a large head on the WHA penetrator (Figure 2) and reducing the eventual depth of penetration.

In this study, the possible benefits of orienting the microstructure of WHAs to augment shear localizations and discard behavior was explored. WHA penetrators were produced with microstructures oriented at different angles with respect to the axis of the penetrator. The influence of microstructural orientation on ballistic performance was assessed in model-scale tests.

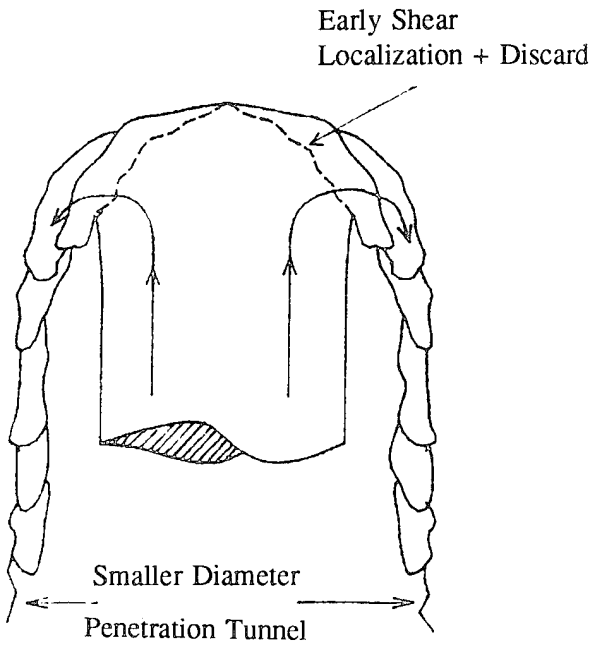

Figure 1. Flow and failure behavior of DU residual penetrators.

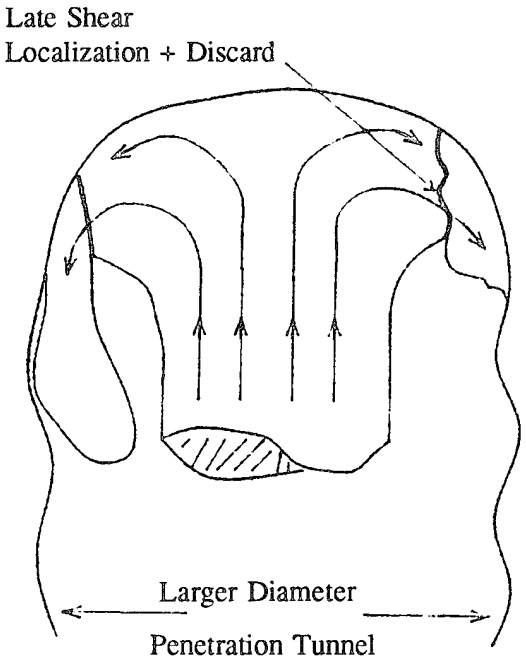

Figure 2. Flow and failure behavior of WHA residual penetrators.

2. MATERIAL PROCESSING

Commercially available WHAs are produced by the liquid-phase sintering of powders of the tungsten and matrix materials (German 1992). The as-sintered microstructure of these conventional WHAs consists of nearly spherical tungsten particles embedded in a metal matrix (typically an alloy of nickel and iron with a significant percentage of tungsten also in solution). The as-sintered WHA bars are usually cold-worked to strengthen the alloy for most penetrator applications. The cold-working is generally accomplished by swaging to reduction-in-areas ranging from 10% to over 30%. The tungsten particles in the microstructure of the swaged alloys are slightly elongated, oriented along the axis of the penetrator.

While the increased strength of the worked WHA is exploited to develop lighter, more efficient sabots and projectile assemblies, varying the strengths, ductilities, and toughnesses of the WHAs with cold-work, via swaging or extrusion, has not resulted in any significant change in ballistic performance of these materials. It was hypothesized that if the WHA microstructure was oriented at an angle to the penetrator axis (Figure 3), it might aid the focus and propagation of adiabatic shear failures within the aligned matrix phase. In this manner, it might be possible to initiate a shear localization and discard behavior similar to that observed for DU and reduce the size of the "mushroomed" head that develops on the WHA penetrator.

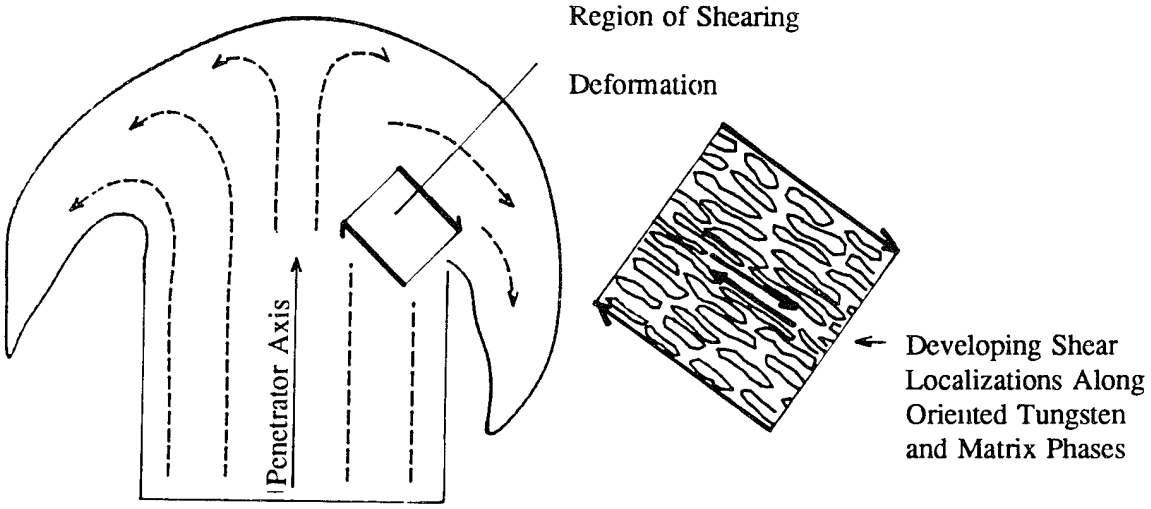

Figure 3. Idealized flow and failure of WHA oriented microstructure.

To produce the oriented microstructure penetrators, a 1-in-thick WHA (90%W-8%Ni-2%Fe) plate was unidirectionally rolled in multiple passes to a final thickness of 0.3 in. This amount of plastic deformation, approximately 80% reduction-in-area, was insufficient to develop any preferred crystallographic orientation (texture) in the WHA composite (Thompson-Russell 1975). However, the microstructure itself was heavily oriented, consisting of tungsten "pancakes" flattened in the plane of the plate and highly elongated in the rolling direction. Sections were then taken from the plate at orientations parallel, perpendicular, and at 30°, 45°, and 60° with respect to the rolling direction. The cross sections were then machined into quarter-scale penetrators. The penetrators were right circular cylinders with a length-to-diameter (L/D) ratio of 15 and a mass of 65 g.

3. BALLISTIC TESTING

All of the ballistic testing of the penetrator materials took place at the U.S Army Research Laboratory's (ARL's) Range 110 indoor facility. The projectiles were placed in a four-piece polypropylux sabot package and push launched from a 26-mm interior diameter (ID) smoothbore gun positioned only 3 m in front of the target. Two pairs of orthogonal x-ray stations captured radiographic images of the penetrator prior to its impact with the target, to measure its striking velocity and its orientation in flight. A second pair of x-ray stations located behind the target recorded images to determine the penetrator's residual velocity and mass. A schematic of the range setup, including x-ray coverage, is given in Figure 4.

Rods of each of the five orientations were fired into large, effectively semi-infinite blocks of rolled homogeneous armor (RHA) at a constant (1,500 m/s) impact velocity. The depth at which each penetrator came to rest in the target served as a measure of its penetration capability. The orientation of the rolling plane in the penetrator cross section could not be controlled in the ballistic firings. After sectioning the target and embedded penetrator along the shot line to determine penetration depth, each residual penetrator was removed from the RHA target. The back end of the rod was then polished and examined to determine the orientation of the rolling plane in the rod. Once determined, the residual penetrator was mounted in bakelite and polished so that a cross section perpendicular to the rolling plane could be examined metallographically.

In addition to the semi-infinite tests, limit velocities were determined for three of the microstructural orientations (parallel, perpendicular, and at 45° to the rolling direction) against a finite RHA target. A limit velocity defines the velocity at which a penetrator will just perforate a given target. All of the

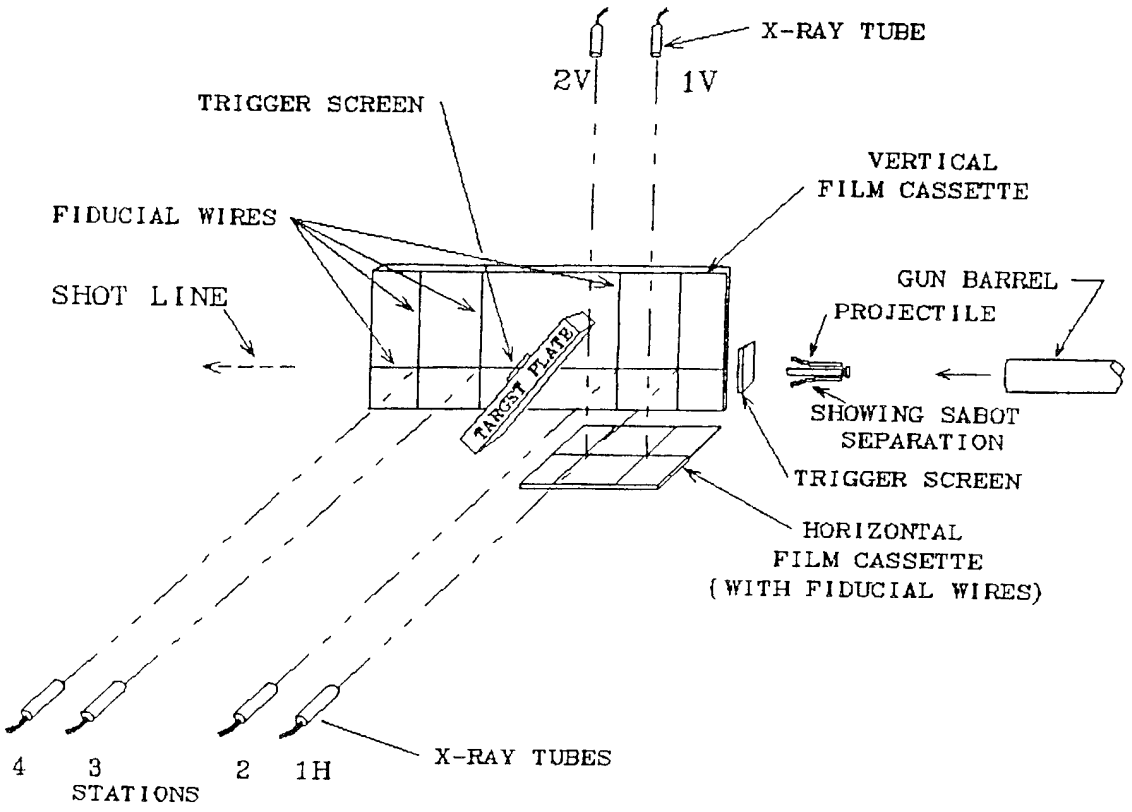

Figure 4. Schematic of range setup.

penetrators were fired into a 3-in monolithic RHA target at 0° obliquity (normal incidence). The limit velocity for each orientation was calculated using a nonlinear least-squares fit to the striking velocity-residual velocity data pairs (Lambert and Jonas 1976) collected from the x-ray images.

Appendix A defines all the headers used in Appendix B. The data collected from all of the individual firings are tabulated in Appendix B. Limit velocity curves are also shown for each series of finite target tests.

4. TEST RESULTS

Table 1 lists the striking velocities and depths of penetration for the semi-infinite tests. Little, if any, difference in penetration performance with microstructural orientation was observed and improvement in penetration due to rod orientation is negligible. In visual examinations, the penetration channels and the residual WHA penetrators looked remarkably similar for all orientations. All of the embedded residual penetrators had large mushroomed heads which were approximately the same size and shape.

Table 1. Ballistic Performance of Oriented Microstructure Penetrators

Microstructure Orientation	3-in RHA at 0° Limit Velocity (m/s)	Semi-Infinite Striking Velocity (m/s)	Depth of Penetration (in)
parallel	1,375	1,500	3.375
30° to rolling direction	—	1,440	3.175
45° to rolling direction	1,373	1,491	3.225
60° to rolling direction	—	1,503	3.225
perpendicular	1,377	1,503	3.325

Table 1 also lists the results of the limit velocity tests against the 3-in RHA targets. There was less than a 5-m/s spread between the limit velocities obtained for the penetrators of three different microstructural orientations, ranging from 1,373 m/s to 1,377 m/s, well within the experimental error of this test method.

5. DISCUSSION

The stresses generated at the interface between penetrator and armor materials greatly exceed the strengths of both materials. The WHA rod is "consumed," inverted, and back-extruded at the penetrator-target interface, as it creates a cavity in the armor steel. The deformation of the penetrator material occurs under high hydrostatic pressures, due to the inertial confinement of the surrounding steel armor, which prevent or suppress fracture failures in the WHA material. The WHA must undergo very large plastic strains before the back-extruding material is finally discarded. A large mushroom forms on the head of the penetrator during this process. It was hoped that aligning the tungsten particles and the soft matrix at an angle with respect to the penetrator axis would change this process of deformation and lead to an earlier failure and discard of material.

A conventionally processed WHA penetrator and a unidirectional-rolled WHA penetrator, embedded in RHA steel from a semi-infinite firing, are compared in Figures 5 and 6, respectively. The original rolling direction in the oriented microstructure WHA penetrator, in Figure 6, was parallel to the axis of the penetrator (0° orientation). In the low magnification views of the residual penetrators, the overall flow

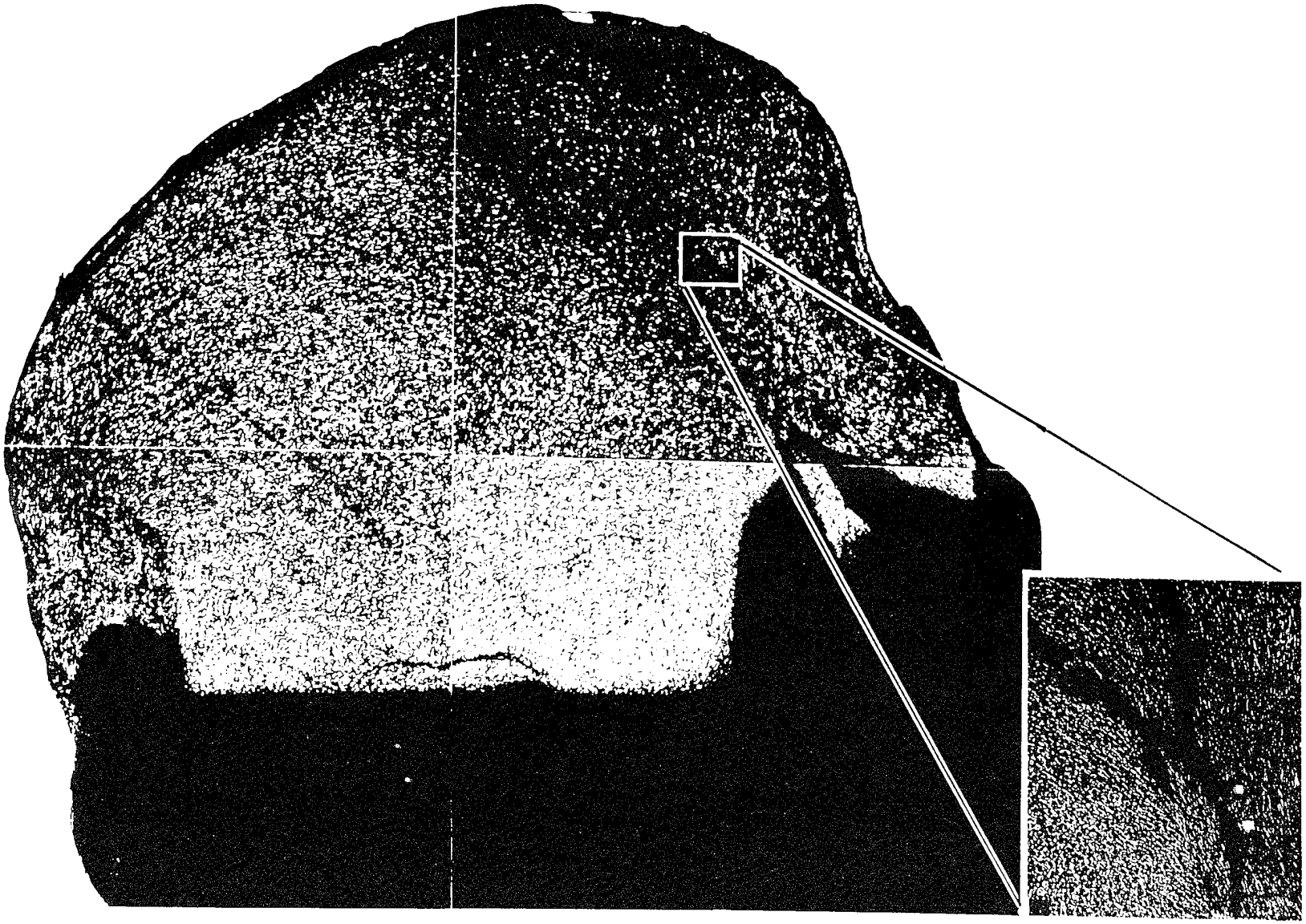

Figure 5. Conventionally processed WHA embedded in RHA.

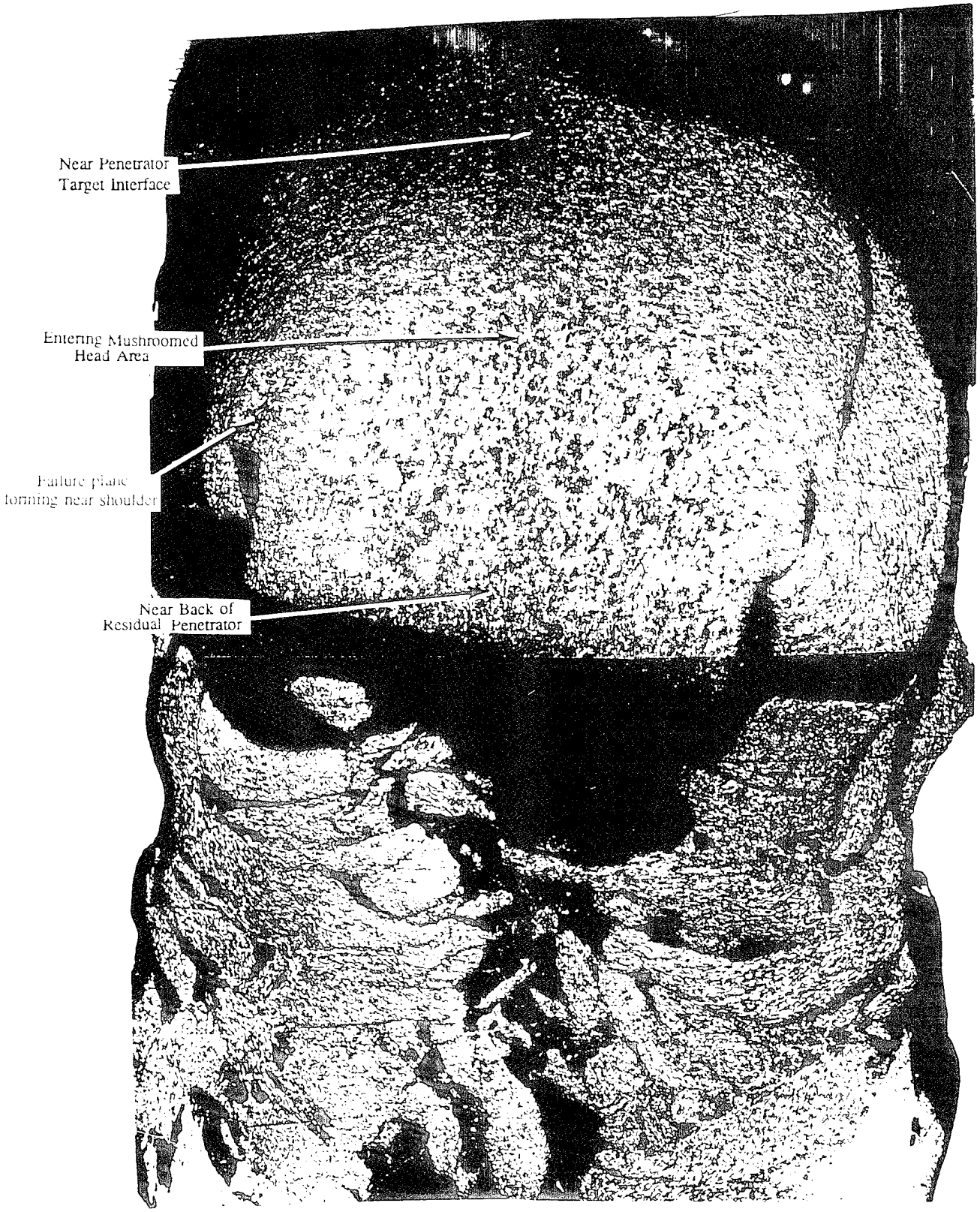

Figure 6. Embedded residual penetrator, original microstructure oriented at 0° to penetrator axis (12.5×).

and failure behaviors of the penetrator materials look very similar. The front of both of the penetrators were back-extruded and eroded away as they penetrated the target. Discarded projectile and armor debris line the walls of the penetration cavity. Both rods exhibit large mushroomed heads.

The distributions and the nature of the deformation within the heads of the penetrators were examined and compared for each of the WHA microstructure orientations. The microstructures were examined in detail at strategic locations in each of the residual penetrators. In Figure 7 (a–c), the condition of the microstructure in the residual 0° orientation rolled WHA penetrator, at the three locations indicated in Figure 6, was studied.

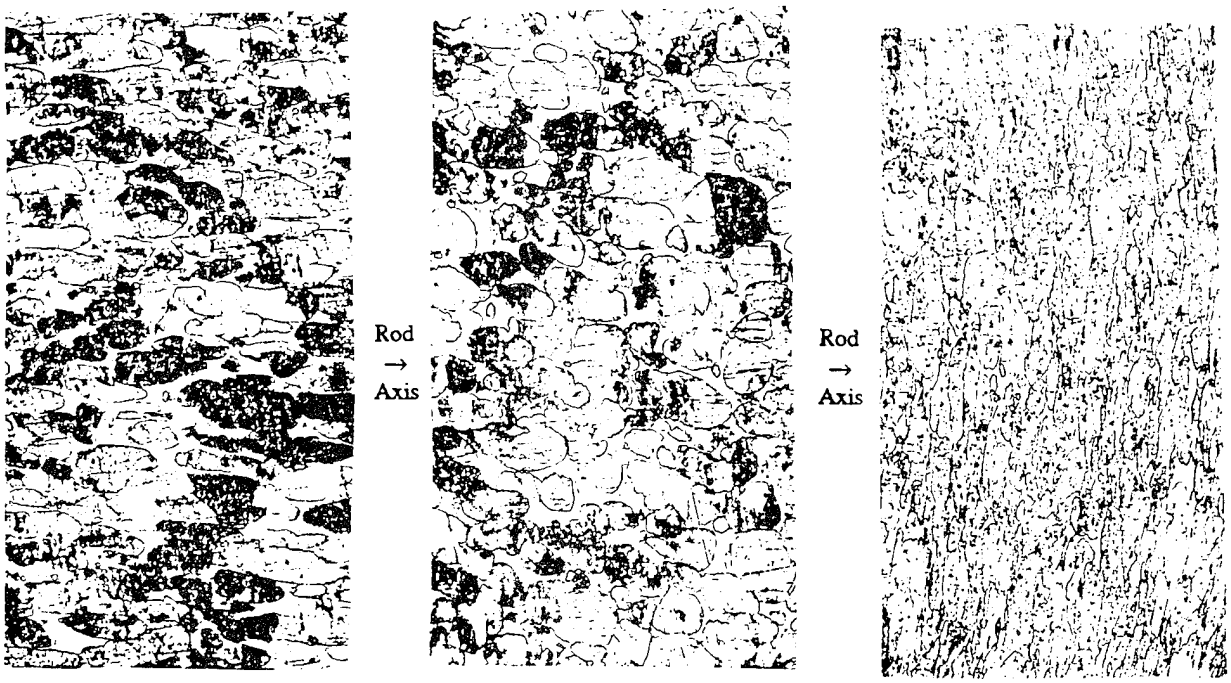

(a) Microstructure near back of residual penetrator.

(b) Microstructure entering mushroomed head area.

(c) Microstructure near penetrator-target interface.

Figure 7. Evolution of deformation in residual penetrator, original microstructure oriented at 0° to penetrator axis (100×).

The rear end of the original long rod penetrator can be clearly identified in Figure 6. The microstructure of the WHA, at a point near the back end of the penetrator, is shown in Figure 7 (a). The aspect ratio of the tungsten particles, elongated parallel to the axis of the rod, are unchanged from those

found in the alloy's original microstructure, indicating that the material underwent little or no deformation at this location. Metallographic examinations at locations within the mushroomed head, however, reveal that the plastic deformation increases steadily as one approaches the penetrator-target interface. As the penetrator material feeds into the mushroomed head, the deformation is primarily compressive and the elongated tungsten grains initially become more circular (Figure 7b). Still closer to the penetrator-target interface, the tungsten grains begin to re-elongate (transverse to the penetrator axis) and start to rotate laterally as the material begins to "turn the corner" and invert (Figure 7c).

A similar evolution of deformation was observed in residual penetrators recovered from tests of rods sectioned from the rolled plate at 90° to the plate's rolling direction (Figure 8). The oblong tungsten particles at the rear of the residual penetrator have essentially the same aspect ratio as the original material cut from the rolled plate (Figure 9a) but are now oriented perpendicular to the rod axis. As one moves forward in the residual penetrator and begins to near the penetrator-target interface, additional plastic strains become evident in the deformation of the microstructure and the tungsten grains become even more elongated than before (Figure 9b). Even closer to the penetrator-target interface, the shape and the orientation of the tungsten grains in the microstructure continue to change as the material begins to invert and flow around the head of the residual penetrator (Figure 9c).

Microstructural examinations of the residual penetrators from tests of rods cut at a 45° orientation with respect to the rolling direction in the plate also revealed similar progression of deformation and failure (Figure 10). In Figure 11a, the elongated original microstructure of the penetrator (at 45° to the axis of the penetrator) can be seen at the rear of the residual penetrator. The microstructure again becomes more elongated closer to the penetrator-target interface (Figures 11b and 11c).

The regions of greatest plastic strain occur near the periphery of the mushroomed head and at the "shoulders" where the penetrator starts to invert. In these areas, localizations begin to form. Figure 12 shows the shoulder of a residual penetrator with a 0° original microstructural orientation. Localizations form and continue to grow and focus until failure planes develop and the penetrator material is discarded. A similar flow, localization, and failure pattern develops in penetrators with 45° and 90° oriented microstructure, Figures 13 and 14, respectively.

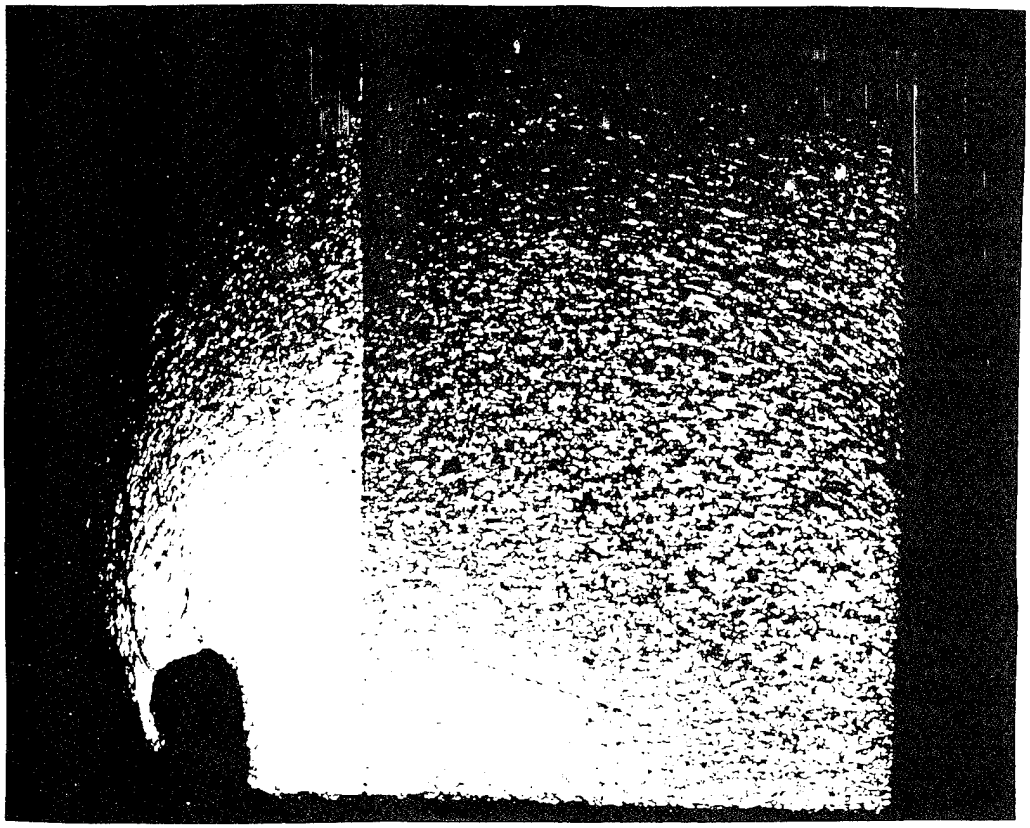

Figure 8. Embedded residual penetrator, original microstructure oriented at 90° to penetrator axis (12.5×).

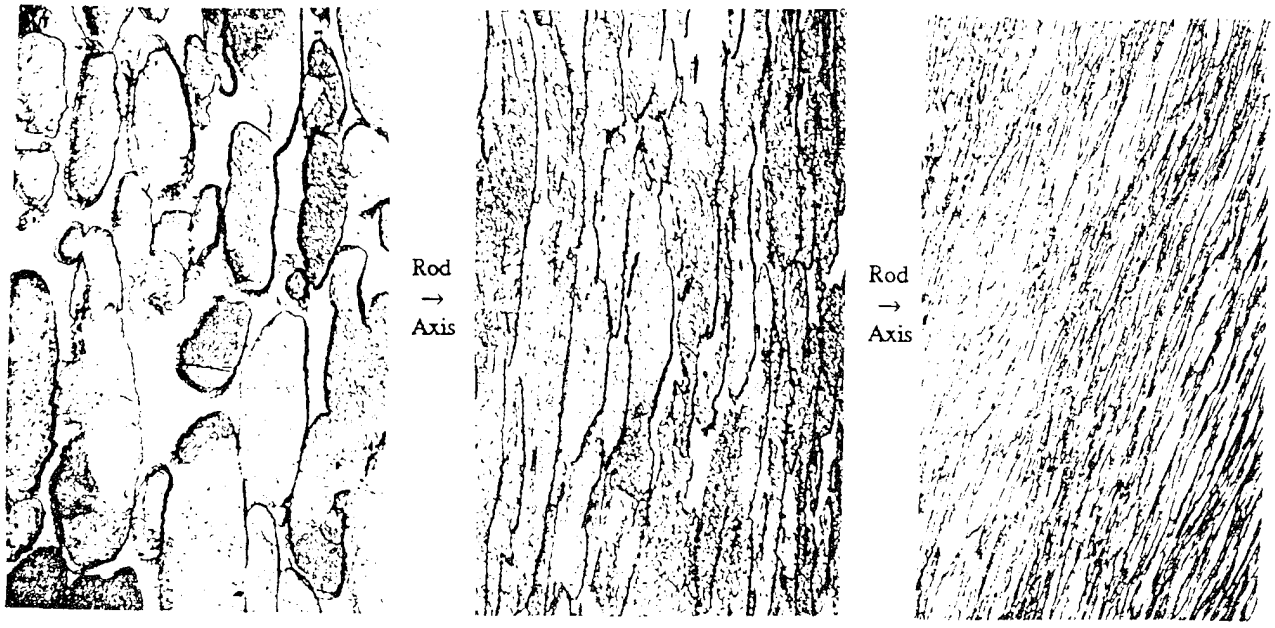

(a) Microstructure near back of residual penetrator.

(b) Microstructure entering mushroomed head area.

(c) Microstructure near penetrator target interface.

Figure 9. Evolution of deformation in residual penetrator, original microstructure oriented at 90° to penetrator axis (250×).

For all of the microstructural orientations, including the 30° and 60° orientations not illustrated in this report, the deformation of the WHA composite in each residual penetrator was continuous and evenly distributed between both tungsten and matrix phases. Localizations, which developed at about the same point in the deformation for all orientations, appeared at the peripheries of the inverted penetrators, and only after the penetrators had developed large mushroomed heads.

Figure 10. Embedded residual penetrator, original microstructure oriented at 45° to penetrator axis (25x).

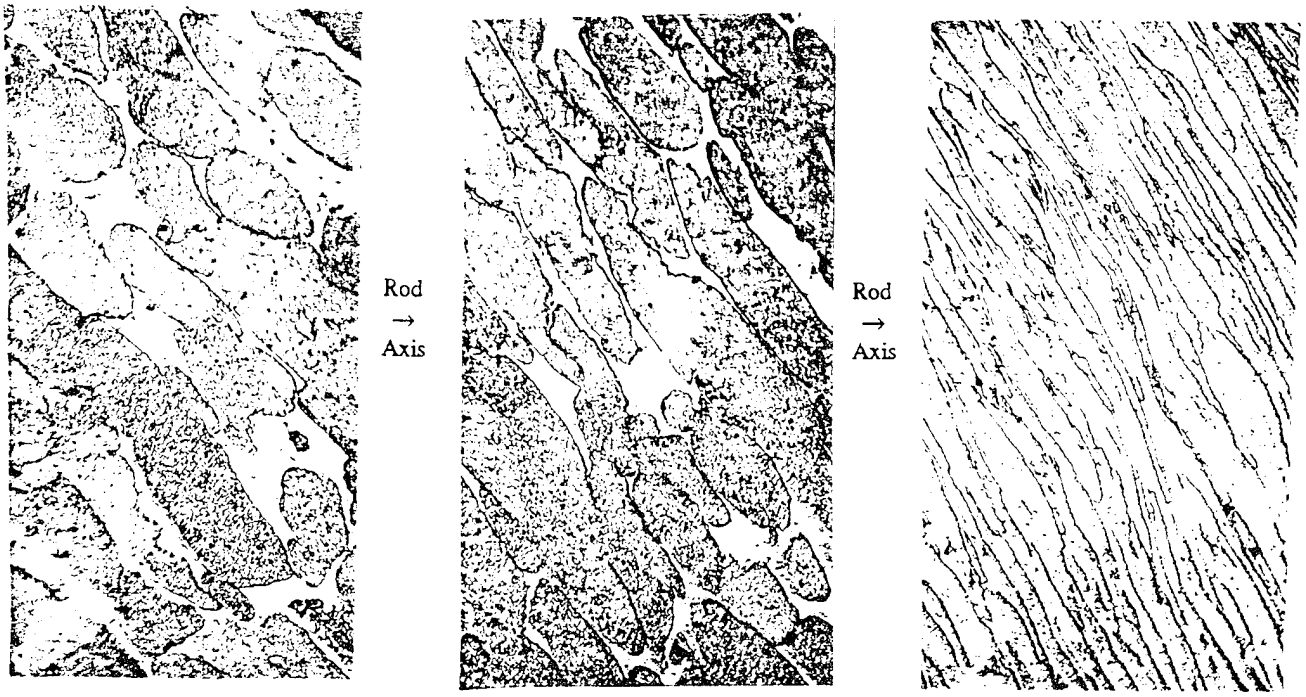

(a) Microstructure near back of residual penetrator.

(b) Microstructure entering mushroomed head area.

(c) Microstructure near penetrator target interface.

Figure 11. Evolution of deformation in residual penetrator, original microstructure oriented at 45° to penetrator axis (250×).

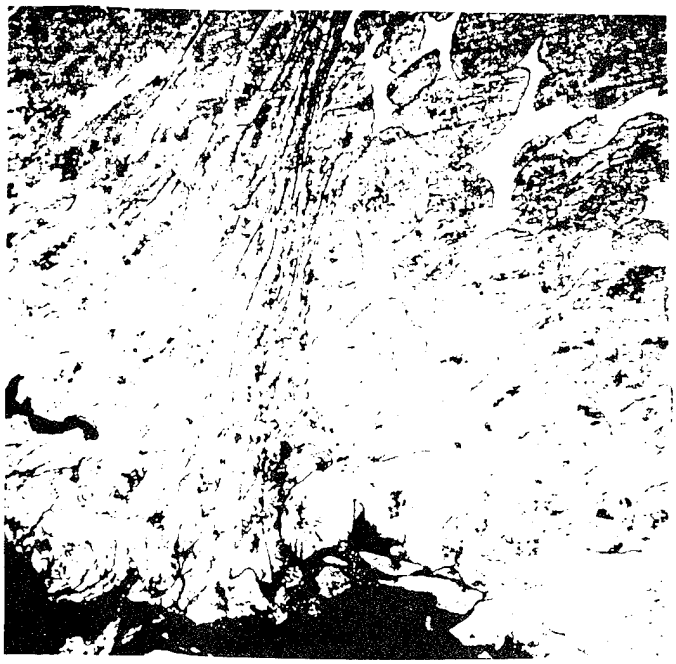

Figure 12. Failure planes forming near shoulders of WHA penetrator, original microstructure oriented at 0° to penetrator axis (250×).

Figure 13. Failure planes forming near shoulders of WHA penetrator, original microstructure oriented at 45° to penetrator axis (250×).

Figure 14. Failure planes forming near shoulders of WHA penetrator, original microstructure oriented at 90° to penetrator axis (250×).

6. CONCLUSIONS

Varying the microstructural orientation of tungsten and matrix phases in a conventional WHA failed to influence the flow and failure behavior of the composite during penetration. The localization of deformation, and the discard of deformed material from the "mushrooming" head of the penetrator, was essentially unchanged. The minimal effects of microstructural orientation on flow and failure behavior may be due in part to the very even distribution of the overall deformation between both tungsten and matrix phases. This approach may yet have some utility, however, in novel tungsten composites designed to minimize these interactions between tungsten and matrix phases.

INTENTIONALLY LEFT BLANK.

7. REFERENCES

German, R. M. "Critical Developments in Tungsten Heavy Alloys." Proceeding from the 1st International Conference on Tungsten and Tungsten Alloys, Arlington, VA, November 1992.

Lambert, J. P., and G. H. Jonas. "Towards Standardization in Terminal Ballistic Testing: Velocity Representation." Report No. 1852 (ADA021389), U.S. Army Ballistic Research Laboratory, Aberdeen Proving Ground, MD, January 1976.

Leonard, W., L. Magness, and D. Kapoor. "Improving Mechanical Properties of Tungsten Heavy Alloy Composites Through Thermomechanical Processing." Proceedings from the 1st International Conference on Tungsten and Tungsten Alloys, Arlington, VA, November 1992.

Magness, L., and T. Farrand. "Deformation Behavior and Its Relationship to the Penetrator Performance of High-Density KE Penetrator Materials." Proceedings from the 1990 Army Science Conference, Durham, NC, May 1990.

Meyer, L., F. Behler, K. Frank, and L. Magness. "Interdependencies Between the Dynamic Mechanical Properties and the Ballistic Behavior of Materials." Proceedings from the 12th International Ballistics Symposium, San Antonio, TX, August 1990.

Thompson-Russell, K. C. "Development of Deformation Texture and Nucleation on Recrystallization in Heavily Deformed Drawn Tungsten Wire." Proceedings from the 4th European Conference on Texture in Metals, Cambridge, UK, July 1975.

Woolsey, P., R. Dowding, K. Tauer, and F. Hodi. "Performance-Property Relationships in Tungsten Alloy Penetrators." Proceedings from the 1st International Conference on Tungsten and Tungsten Alloys, Arlington, VA, November 1992.

INTENTIONALLY LEFT BLANK.

APPENDIX A:

EXPLANATION OF INDIVIDUAL FIRING DATA

INTENTIONALLY LEFT BLANK.

The following is a description of the table headings and columns which are used in the individual shot data for each test series detailed in Appendix B.

The "test series label" at the top of each table describes the particular penetrator material, penetrator geometry, and the particular target common to the firings listed below the heading. Each "test series table" is organized into three subtables. The uppermost subtable, essentially a "black-box" description, lists the most important measurable preimpact parameters, such as the striking velocity, mass, yaw, and pitch, followed by the most important postimpact data, including the residual penetrator's mass, velocity, and flight direction.

The other two subtables tabulate additional postimpact data such as the target plug mass and velocity; the entrance, exit, and mid-plate dimensions of the perforation hole; and other behind-armor debris measures for single plate targets. Figures A-1–A-4 illustrate many of the measurable quantities for single plate targets.

An additional set of data, generated to determine characteristics of penetration into semi-infinite armor, may also be included in Appendix B. The values listed in this table are obtained by sectioning the semi-infinite plate along the centerline of the penetration hole. This table is divided into two subtables, the first is the "black-box" table, and the other contains secondary measures of the penetration tunnel. Figure A-5 is a schematic of the sectioned penetration tunnel and its related measures.

Below is an alphabetical listing of the abbreviations used as column headings in each of the subtables, with a definition of each term and a brief description of how it is measured. Also included are some of the abbreviations used for the entries in the columns. Some of the listings below may not have entries in the test series tables generated as part of this report.

A - an adjustable parameter in the limit velocity functional formulation, $V_r = A\,(V_s^p - V_L^p)^{1/p}$, where A is the slope of the asymptote of the fitted curve, restricted to $A < 1$.

Alpha - α, the striking pitch, orientation of the projectile relative to its flight path, measured in the vertical plane, degrees (see Figure A-1).

Alpha1 - (Alpha2) - $\alpha 1$ ($\alpha 2$), pitch of projectile after perforating the first (second) plate of spaced array target, relative to projectile's flight path, degrees.

AlphaR - αR, the pitch of final residual penetrator, relative to its residual flight path; the entry NA appears if the residual penetrator is tumbling rapidly, degrees (see Figure A-1).

Area - the cross-sectional area of the penetrator, used for comparisons in the semi-infinite data, square centimeters.

Area hole - the average cross-sectional area of the hole produced in semi-infinite test, measured by using the diameter of the sectioned armor and assuming a circular tunnel, square centimeters (see Figure A-5).

Beta - β, the striking yaw, orientation of the projectile relative to its flight path, measured in the horizontal plane, degrees.

BG/L or Blg. - height of lip on the exit hole or bulge height, height above the rear surface of the plate, measured perpendicular to surface, centimeters (see Figures A-2, A-3).

BHN - Brinell Hardness of monolithic target plate.

BHN1, BHN2, BHN3 - Brinell Hardness of first, second, and third plates of spaced array target.

BlgL - bulge length, length of rear surface bulge of finite monolithic target or of last plate in spaced array target, centimeters (see Figure A-2).

BlgW - bulge width, width of rear surface bulge of finite monolithic target or of last plate in spaced array target, centimeters.

CenL - center hole length, length of penetration hole at midthickness in the plate, measured in the plane of target, centimeters (see Figure A-3).

CenW - center hole width, width of penetration hole at midthickness in the plate, centimeters (see Figure A-3).

CL PL#1,2,3 - center hole length in first (second, third) plate of spaced array target, length of penetration hole at midthickness in the plate, centimeters.

CW PL#1,2,3 - center hole width in first (second, third) plate of spaced array target, width of penetration hole at midthickness in the plate, centimeters.

CoFS - center of fragment spray angle, the average direction of the behind-armor debris, measured relative to the penetrator's original flight path, estimated from the behind-armor radiographs in the vertical plane, degrees (see Figure A-4).

Cone - cone angle or enclosed spray angle, angle in space which encloses the behind-armor debris cloud, estimated from behind-armor radiographs in the vertical plane, degrees (see Figure A-4).

Dt/Dp - Diameter of the tunnel produced in semi-infinite targets divided by the original diameter of the penetrator, nondimensional.

EHL - exit hole length, length of exit hole on rear surface of plate, measured in plane of plate, centimeters (see Figure A-3).

EHW - exit hole width, width of exit hole on rear surface of plate, measured in plane of plate, centimeters (see Figure A-3).

EntHL - entrance hole length, length of entrance hole on front surface of target, measured in plane of target plate, centimeters (see Figure A-3).

EntW - entrance hole width, width of entrance hole on front surface of target, measured in plane of target plate, centimeters (see Figure A-3).

EtaP - ηp, departure angle of target plug, measured relative to penetrator's original flight path, from x-ray images in the vertical plane, degrees (see Figure A-1).

ETA1 (2, 3) - $\eta 1$ ($\eta 2$, $\eta 3$), departure angle of residual penetrator after exiting the first (second, third) plate of a spaced array target, measured relative to penetrator's original flight path, from x-ray images in the vertical plane, degrees.

F - fineness ratio, the length-to-diameter (L/D) ratio of the penetrator.

Gamma - γ, total solid angle orientation of the striking penetrator to its initial flight path ($\alpha^2 + \beta^2 = \gamma^2$), degrees.

K.E. - kinetic energy, the kinetic energy of the round impacting the semi-infinite target, joules.

KE/A - kinetic energy divided by cross-sectional area of penetrator, the energy per area impacting semi-infinite armor, joules/square centimeter.

KE/Vt - kinetic energy divided by total volume, the energy impacting the armor divided by the total volume of the tunnel generated while penetrating semi-infinite armor, joules/cubic centimeter.

LP - length of target plug, average dimension of plug, oriented to correspond to exit hole length in target, where applicable, used in residual plug mass estimates, centimeters.

M/A - mass of penetrator divided by cross-sectional area of penetrator, used primarily in semi-infinite data, grams/square centimeter.

M/A hole - mass of penetrator divided by cross-sectional area of hole generated in semi-infinite penetration, grams/square centimeter.

MPL - mass of target plug or plugs, estimated from behind-armor radiographic images, grams (see Figure A-1).

MPr - recovered plug mass or masses, actual mass of plug recovered after a test firing, compared with MPL value as a check on estimation accuracy, grams.

Mr - mass of residual penetrator or residual penetrators, estimated from images in behind-armor radiographs, grams (see Figure A-1).

MR1 (2) - residual mass of penetrator after perforating the first (second) plate of a spaced array target, estimated from radiographic images, grams.

M.R. Dia - maximum rod diameter, maximum diameter of the mushroomed portion of the final residual penetrator, if applicable, centimeters.

M. rec - mass of recovered residual penetrator, compared with Mr values as a check on estimation accuracy, grams.

Ms - mass of penetrator before target impact, grams (see Figure A-1).

NC - not calculated.

NM - not measured.

NR - not recovered.

No. of Pcs. - number of major identifiable final residual penetrator pieces seen in behind-armor radiographic images. The breakup behavior of the penetrator is indicated by a number code:

1 - one whole piece
21 - two pieces, fracture at nose section
22 - two pieces, fracture at tail section
23 - two pieces, fracture at midlength
31 - three pieces, fracture at nose section
32 - three pieces, fracture at tail section
33 - three pieces, evenly distributed fractures
Frag - many pieces, too small to accurately measure.

#Pc1 (2) - number of major residual penetrator pieces after first (second) plate of spaced array target, uses same number code as No. of Pcs. on previous page, with addition of 40 - four or more pieces.

P - an adjustable parameter of the limit velocity determination equation $V_r = A (V_s^P - V_L^P)1/P$, where P is the power determining how rapidly the fitted curve rises to the asymptote, arbitrarily restricted to $2 < P < 8$ values.

Pen., Pene or Pn - penetration depth into target plate (finite, semi-infinite, or last plate of spaced array target), for partial penetrations measured normal to the plate surface, centimeters (see Figure A-2 and A-5).

P/L - penetration depth divided by original length of penetrator, nondimensional term used in normalizing the depth of penetration into semi-infinite armor.

ρlv^2 - density times the length times the velocity squared of the penetrator, a term used to characterize the impacting penetrator into a semi-infinite plate, grams/square second.

Rise - target plate rise, rise of the front surface of the target plate encountered after the penetrator has impacted the semi-infinite armor, centimeters (see Figure A-5).

Rot - rotation, the apparent change in pitch of the final residual penetrator between the two behind-armor x-ray images, indicative of penetrator tumbling, degrees.

RotR 1 (2) - rotation rate (pitch rate) of the residual penetrator after the first (second) plate of spaced array target, using the convention that rotation of the nose of the rod toward the target normal is positive, degrees/second.

S - standard deviation, measure of the data spread of Vs, Vr data pairs from the fitted Vs-Vr curve, measured on the Vr axis (vertical) only, meters/second.

Shot No. or Sh.# - shot number, the individual test firing identification number, a negative number, indicates that the resulting data was not considered a "fair hit" and, therefore, not used in the limit velocity or V-50 determination.

Time - time between the two behind-armor x-ray flashes, microseconds.

Th. - target plug thickness, the thickness of the rear surface of the target plate that was removed as a plug, estimated from x-ray images of the target plug, used in plug mass estimates, centimeters.

Vol Base (Tot) - volume of the penetration hole within target (total volume of penetration tunnel, including portion created from Rise), estimated volume of the penetration tunnel created in semi-infinite armor, determined by estimating area of half section and assuming the tunnel was circular, cubic centimeters (see Figure A-5).

Vpl - velocity of the target plug, as measured in the vertical plane, calculated from behind-armor radiographic images, meters/second (see Figure A-1).

Vr - velocity of the final residual penetrator, measured in the vertical plane, calculated from behind-armor radiographic images, meters/second (see Figure A-1).

Vr1 (2) - velocity of the residual penetrator after the first (second) plate of spaced array target, meters/second.

Vs - striking velocity of penetrator, calculated from pre-impact images of penetrator in both vertical and horizontal planes, meters/second (see Figure A-1).

W.p - width of target plug, average dimension of plug, oriented to correspond to exit hole width in target plate where applicable, estimated from x-ray images of target plug, used in plug mass estimates, centimeters.

Wt. L - net weight loss of target plate, determined by measuring weight of target plate before and after each test firing, grams.

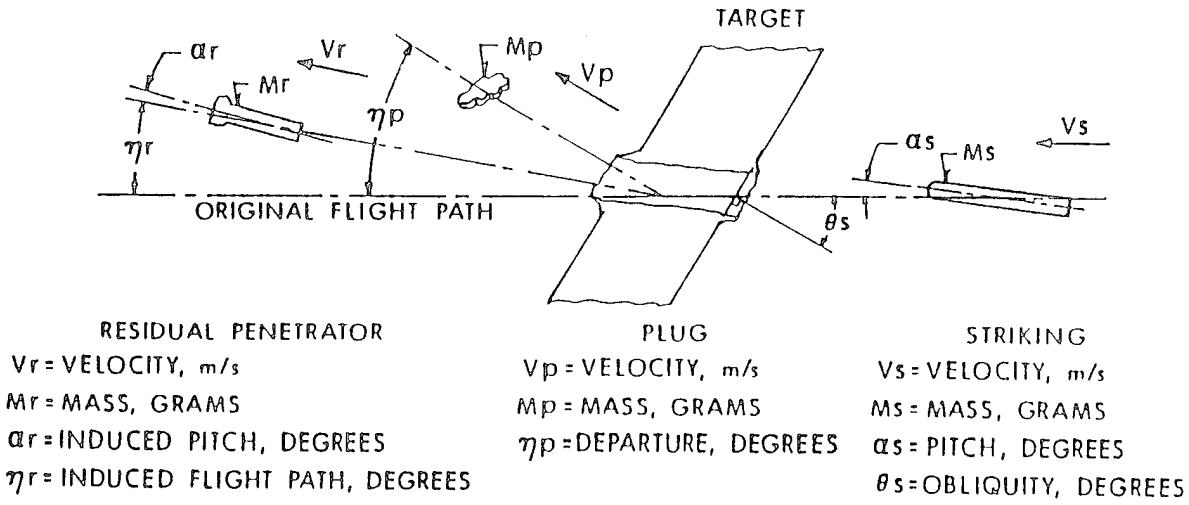

Figure A-1. Illustration of primary preimpact and postimpact radiographic measures.

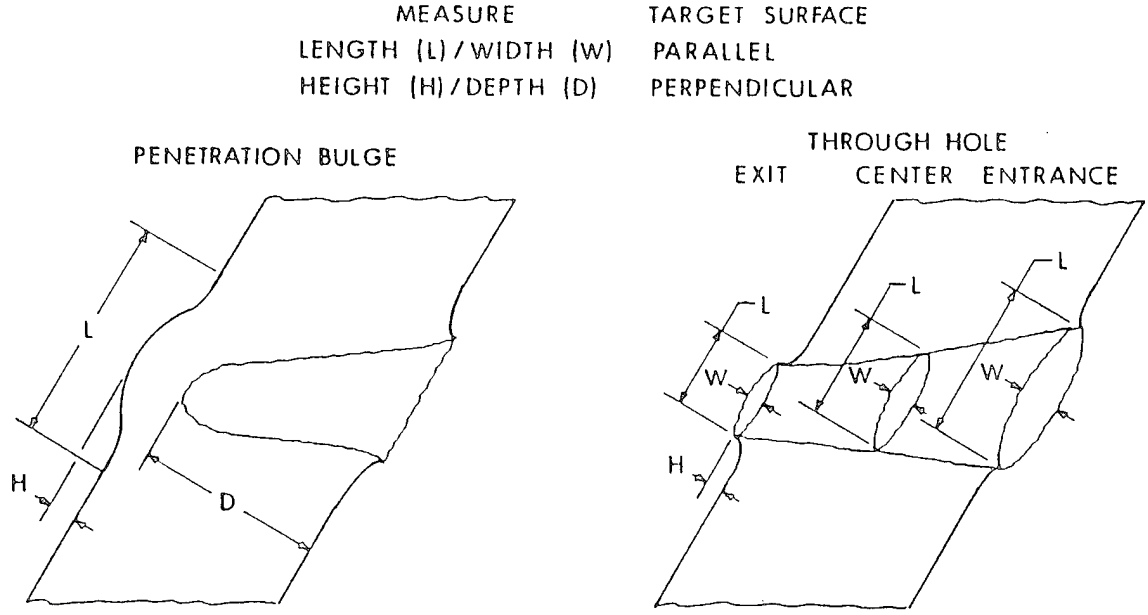

Figure A-2. Illustration of target plate measures - partial penetration.

Figure A-3. Illustration of target plate measures - complete penetration.

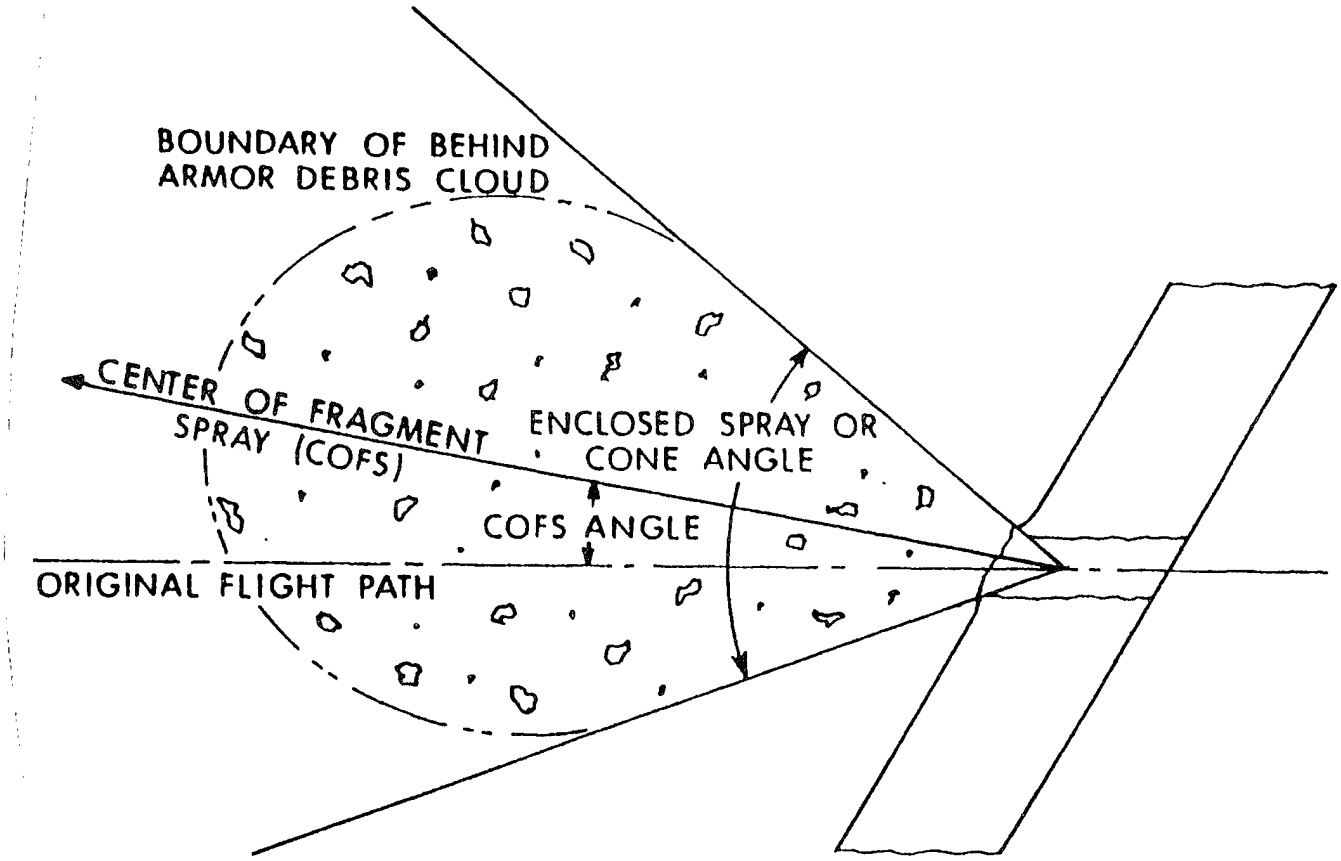

Figure A-4. Illustration of radiographic behind-armor debris measures.

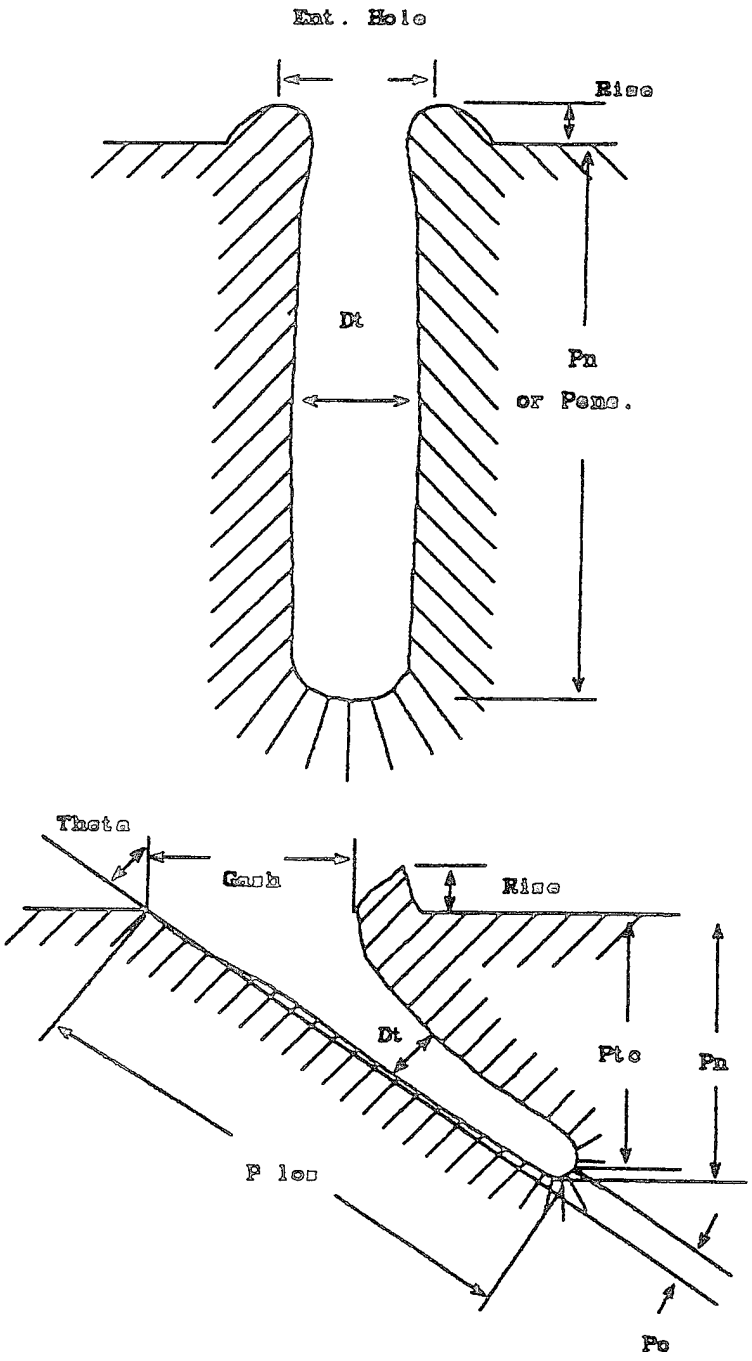

Figure A-5. Illustration of penetration measures in semi-infinite targets.

APPENDIX B:

SHOT DATA SUMMARY TABLES

INTENTIONALLY LEFT BLANK.

Table B-1. Individual Shot Data for Penetrators Oriented at 0° to Rolling Direction vs. 3-in RHA at 0°

Series Fired 10 - 1991

Limit Velocity = 1375 A= .98 P= 2.59 S= 109

Sh.#	Alpha (deg)	Beta (deg)	Gamma (deg)	Vs (m/s)	Ms (g)	EtaR (deg)	AlphaR (deg)	Vr (m/s)	Mr (g)	Pen. (cm)
4184	0.75U	0.50L	0.90	1362	65.21	NA	NA	0	0.00	2.7
4185	0.50U	0.00	0.50	1339	65.16	NA	NA	0	0.00	NM
4186	0.25U	1.25L	1.35	1382	65.15	14.8D	NA	360	4.69	CP
4187	0.00	0.75L	0.75	1378	65.16	NA	NA	0	0.00	4.4
4188	1.00D	1.00L	1.41	1402	65.12	0.4D	NA	333	6.92	CP
4190	0.00	0.25R	0.25	1461	64.96	0.4D	NA	861	9.38	CP
4203	0.75U	0.25R	0.79	1376	64.96	26.0D	NA	114	6.43	CP

Sh.#	M.rec (g)	EtaP (deg)	Vpl (m/s)	Mpl (g)	Mpr (g)	L.p (	W.p cm	Th.)	EHL (cm)	EHW (cm)	Blg (cm)	Wt.L (g)
4184	0.00	NA	0	0.00	0.00	0.0	0.0	0.0	0.0	0.0	0.8	NR.
	BHN= 340											
4185	0.00	NA	0	0.00	0.00	0.0	0.0	0.0	0.0	0.0	0.7	NR.
	BHN= 340											
4186	None	0.0	Lost 111	Lost Lost	None None	----NM----			1.8	0.9	NR.	0
	BHN= 340											
4187	0.00	NA	0	0.00	0.00	0.0	0.0	0.0	0.0	0.0	1.0	0
	BHN= 340											
4188	None	23.3D	219	9.39	None	1.4	1.2	0.7	1.7	1.3	0.0	0
	BHN= 340											
4190	None	0.0	0	0.00	0.00	0.0	0.0	0.0	2.1	1.8	0.0	0
	BHN= 340											
4203	None	41.8D	127	6.41	0.00	1.1	1.0	0.7	1.0	1.0	0.0	0
	BHN= 340											

Table B-1. Individual Shot Data for Penetrators Oriented at 0° to Rolling Direction vs. 3-in RHA at 0° (continued)

Sh.#	Cone (deg)	CoFS (deg)	EntHL (cm)	EntW (cm)	CenL (cm)	CenW (cm)	#Pcs.	M.R.Dia. (inch)	BL (cm)	BW (cm)
4184	NA	NA	1.2	1.2	NA	NA	PP	PP	3.6	3.6
4185	NA	NA	3.3	1.8	NM	NM	PP	PP	3.5	3.5
4186	0.0	0.0	1.1	1.5	0.9	1.3	1	Lost	NM	NM
4187	NA	NA	3.5	2.3	NM	NM	PP	PP	1.0	3.3
4188	0.0	0.0	2.0	3.3	1.1	0.8	1	0.00	0.0	0.0
4190	0.0	0.0	3.1	3.8	1.5	1.5	1	0.00	0.0	0.0
4203	0.0	0.0	1.3	1.3	0.0	0.0	1	0.00	0.0	0.0

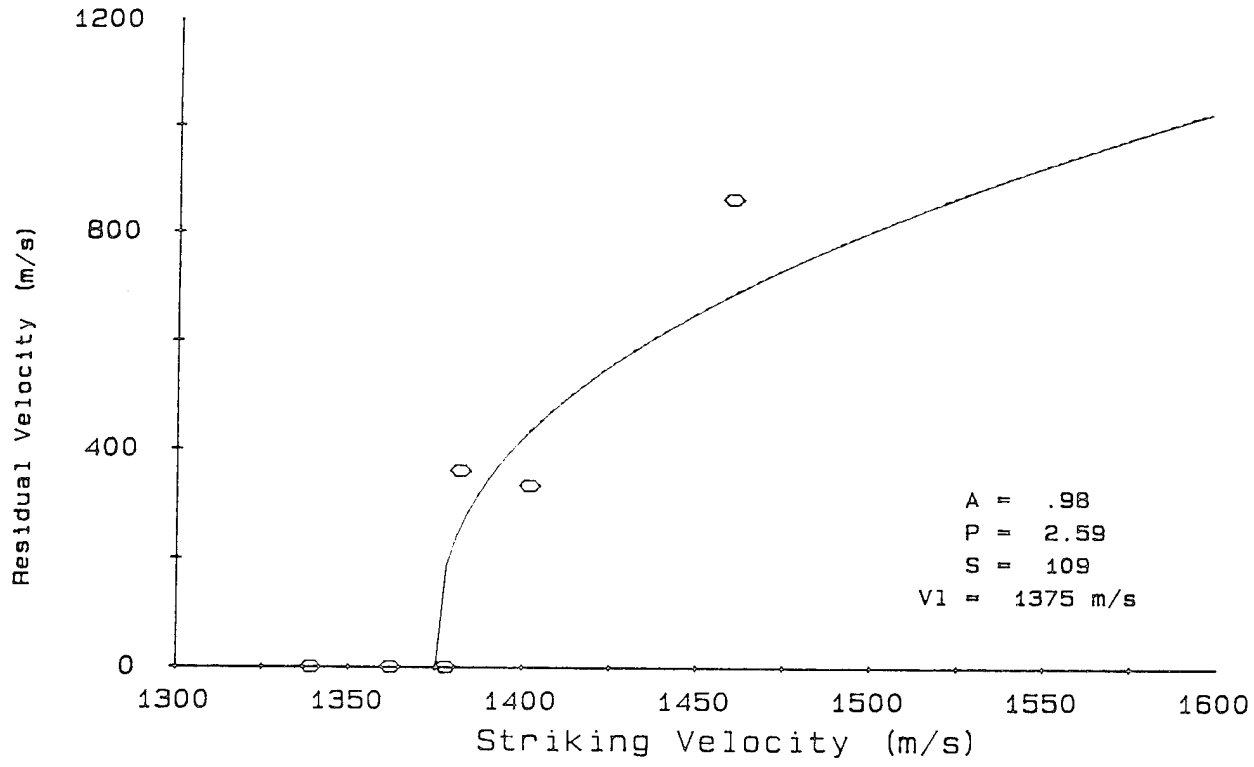

Figure B-1. Vs-Vr curve for penetrators oriented at 0° to rolling direction vs. 3-in RHA at 0°.

Table B-2. Individual Shot Data for Penetrators Oriented at 0° to Rolling Direction vs. Semi-Infinite RHA

Series Fired 5 - 1991
L/D = 15 Density is 17.2

Sh.#	Gamma (deg)	Vs (m/s)	Ms (g)	K.E. (J)	Area (scm)	M/A (g/scm)	KE/A (J/scm)	Norm P/L	Norm Pene. (mm)
4178	0.90	1500	65.08	73215	0.369	176	198205	0.83	85.7

Sh.#	Rise (cm)	Vol base (cc)	Vol total (cc)	KE/Vt (J/cc)	KE/Vb (J/cc)	plV^2 *10^6	Dt/Dp	Area hole (scm)	M/A hole (g/scm)
4178	0.57	9.28	9.85	7433	7890	398	1.66	1.02	63.76

BHN= 269

Table B-3. Individual Shot Data for Penetrators Oriented at 30° to Rolling Direction vs. Semi-Infinite RHA

Series Fired 5 - 1991
L/D = 15 Density is 17.2

Sh.#	Gamma (deg)	Vs (m/s)	Ms (g)	K.E. (J)	Area (scm)	M/A (g/scm)	KE/A (J/scm)	Norm P/L	Norm Pene. (mm)
4174	0.50	1440	64.81	67195	0.368	176	182584	0.78	80.6

Sh.#	Rise (cm)	Vol base (cc)	Vol total (cc)	KE/Vt (J/cc)	KE/Vb (J/cc)	plV^2 *10^6	Dt/Dp	Area hole (scm)	M/A hole (g/scm)
4174	0.51	8.28	11.28	5957	8115	367	1.64	0.99	65.78

BHN= 255

Table B-4. Individual Shot Data for Penetrators Oriented at 45° to Rolling Direction vs. 3-in RHA at 0°

Series Fired 10 - 1991
Limit Velocity = 1373 A= .98 P= 3.09 S= 17

Sh.#	Alpha (deg)	Beta (deg)	Gamma (deg)	Vs (m/s)	Ms (g)	EtaR (deg)	AlphaR (deg)	Vr (m/s)	Mr (g)	Pen. (cm)
-4191	2.00U	0.25R	2.06	1201	64.59	NA	NA	0	0.00	NM
4192	0.25D	1.00R	1.12	1365	64.47	NA	NA	0	0.00	0.0
4193	0.75U	1.00L	1.25	1395	64.33	5.5D	NA	527	7.99	CP
4194	0.75U	0.75L	1.06	1375	64.37	2.0U	NA	240	7.13	CP
4195	1.00U	0.50L	1.12	1370	63.64	NA	NA	0	0.00	0.0
4196	0.00	1.00L	1.00	1459	64.58	0.1U	NA	865	9.94	CP

Sh.#	M.rec (g)	EtaP (deg)	Vpl (m/s)	Mpl (g)	Mpr (g)	L.p (	W.p cm	Th.)	EHL (cm)	EHW (cm)	Blg (cm)	Wt.L (g)
-4191	0.00	NA	0	0.00	0.00	0.0	0.0	0.0	0.0	0.0	0.9	0
	BHN= 340											
4192	0.00	NA	0	0.00	0.00	0.0	0.0	0.0	0.0	0.0	1.2	0
	BHN= 340											
4193	0.00	17.1U	425	3.32	0.00	1.0	0.8	0.5	1.1	1.5	0.0	0
	BHN= 340											
4194	0.00	0.0	0	0.00	0.00	0.0	0.0	0.0	1.8	1.0	0.0	0
	BHN= 340											
4195	0.00	NA	0	0.00	0.00	0.0	0.0	0.0	0.0	0.0	1.1	0
	BHN= 340											
4196	0.00	0.0	0	0.00	0.00	0.0	0.0	0.0	2.3	2.3	0.0	0
	BHN= 340											

Sh.#	Cone (deg)	CoFS (deg)	EntHL (cm)	EntW (cm)	CenL (cm)	CenW (cm)	#Pcs.	M.R.Dia. (inch)	BL (cm)	BW (cm)
-4191	NA	NA	3.7	3.2	NA	NA	PP	PP	3.3	3.3
4192	NA	NA	2.9	2.7	NA	NA	PP	PP	3.2	3.2
4193	0.0	0.0	3.7	2.7	1.0	1.2	1	0.00	0.0	0.0
4194	0.0	0.0	3.5	1.7	1.0	1.0	1	0.00	0.0	0.0
4195	NA	NA	1.1	1.8	NA	NA	PP	PP	3.5	3.0
4196	0.0	0.0	1.0	1.0	1.5	1.5	1	0.00	0.0	0.0

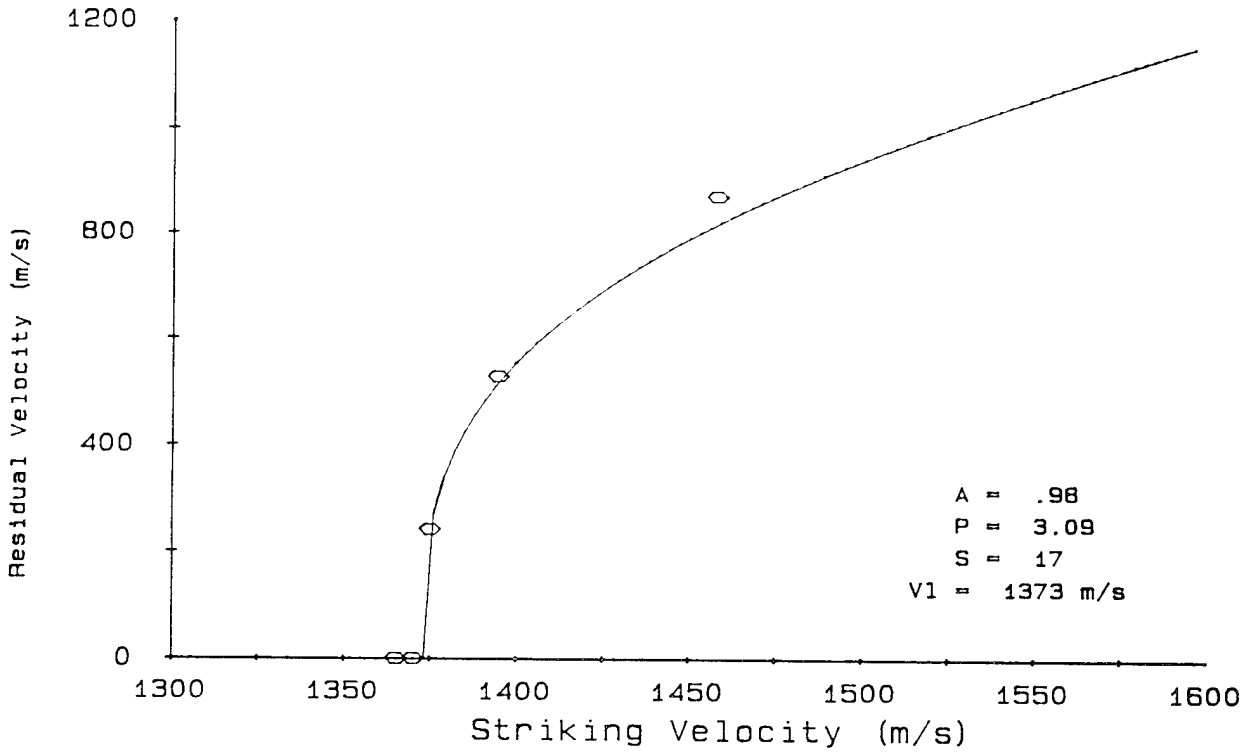

Figure B-2. Vs-Vr curve for penetrators oriented at 45° to rolling direction vs. 3-in RHA at 0°.

Table B-5. Individual Shot Data for Penetrators Oriented at 45° to Rolling Direction vs. Semi-Infinite RHA

Series Fired 5 - 1991
L/D = 15 Density is 17.2

Sh.#	Gamma (deg)	Vs (m/s)	Ms (g)	K.E. (J)	Area (scm)	M/A (g/scm)	KE/A (J/scm)	Norm P/L	Norm Pene. (mm)
4175	1.00	1491	64.70	71917	0.368	176	195414	0.80	81.9

Sh.#	Rise (cm)	Vol base (cc)	Vol total (cc)	KE/Vt (J/cc)	KE/Vb (J/cc)	plV^2 *10^6	Dt/Dp	Area hole (scm)	M/A hole (g/scm)
4175	0.57	9.54	10.17	7071	7538	394	1.75	1.13	57.21
	BHN= 269								

Table B-6. Individual Shot Data for Penetrators Oriented at 60° to Rolling Direction vs. Semi-Infinite RHA

Series Fired 5 - 1991
L/D = 15 Density is 17.2

Sh.#	Gamma (deg)	Vs (m/s)	Ms (g)	K.E. (J)	Area (scm)	M/A (g/scm)	KE/A (J/scm)	Norm P/L	Norm Pene. (mm)
4176	0.90	1503	64.00	72288	0.369	173	195697	0.80	81.9

Sh.#	Rise (cm)	Vol base (cc)	Vol total (cc)	KE/Vt (J/cc)	KE/Vb (J/cc)	plV^2 *10^6	Dt/Dp	Area hole (scm)	M/A hole (g/scm)
4176	0.57	7.41	7.90	9150	9756	400	1.53	0.87	73.91
	BHN= 269								

Table B-7. Individual Shot Data for Penetrators Oriented at 90° to Rolling Direction vs. 3-in RHA at 0°

Series Fired 10 - 1991

Limit Velocity = 1377 A= .99 P= 3.29 S= 67

Sh.#	Alpha (deg)	Beta (deg)	Gamma (deg)	Vs (m/s)	Ms (g)	EtaR (deg)	AlphaR (deg)	Vr (m/s)	Mr (g)	Pen. (cm)
-4197	0.25D	1.75L	1.77	1370	64.32	NA	NA	0	0.00	NM
4198	0.50U	0.75L	0.90	1400	64.95	0.5U	NA	709	9.12	CP
-4199	0.25D	2.25L	2.26	1379	64.28	13.4D	NA	115	Lost	CP
4200	0.50U	1.00R	1.12	1395	64.26	3.1D	NA	467	7.60	CP
4201	1.00U	0.25R	1.03	1379	64.27	9.2U	NA	280	7.48	CP
4202	Lost	Lost	Lost	Lost	64.22	0.5D	NA	861	10.52	CP
4206	1.00D	0.75R	1.25	1356	64.40	NA	NA	0	Lost	0.0
-4207	2.50U	0.25R	2.51	1383	64.99	0.2D	NA	213	4.36	CP
4208	1.00D	0.00	1.00	13	64.85	NA	NA	0	0.00	3.9
-4209	1.00D	1.75L	2.02	1451	64.96	1.1D	NA	902	10.76	CP

Sh.#	M.rec (g)	EtaP (deg)	Vpl (m/s)	Mpl (g)	Mpr (g)	L.p (	W.p cm	Th.)	EHL (cm)	EHW (cm)	Blg (cm)	Wt.L (g)
-4197	0.00	NA	0	0.00	0.00	0.0	0.0	0.0	0.0	0.0	0.811111	
	BHN= 340											
4198	None	0.0	0	0.00	0.00	0.0	0.0	0.0	2.1	1.9	0.0	0
	BHN= 340											
-4199	0.00	0.0	0	0.00	0.00	0.0	0.0	0.0	1.1	1.6	0.0	0
	BHN= 340											
4200	0.00	46.7D	175	3.36	0.00	1.1	0.7	0.6	1.2	1.1	0.0	0
	BHN= 340											
4201	0.00	15.3U	268	3.71	0.00	1.1	0.8	0.6	1.2	0.9	0.0	0
	BHN= 340											
4202	0.00	0.0	0	0.00	0.00	0.0	0.0	0.0	2.0	2.0	0.0	0
	BHN= 340											
4206	None	NA	0	0.00	0.00	0.0	0.0	0.0	0.0	0.0	0.9	0
	BHN= 340											
-4207	0.00	5.0D	219	7.46	0.00	0.9	1.5	0.7	1.5	1.1	0.0	0
	BHN= 340											
4208	0.00	NA	0	0.00	0.00	0.0	0.0	0.0	0.0	0.0	1.2	0
	BHN= 340											
-4209	0.00	0.0	0	0.00	0.00	0.0	0.0	0.0	2.2	2.1	0.0	0
	BHN= 340											

Table B-7. Individual Shot Data for Penetrators Oriented at 90° to Rolling Direction vs. 3-in RHA at 0° (continued)

Sh.#	Cone (deg)	CoFS (deg)	EntHL (cm)	EntW (cm)	CenL (cm)	CenW (cm)	#Pcs.	M.R.Dia. (inch)	BL (cm)	BW (cm)
-4197	NA	NA	NM	NM	NM	NM	PP	PP	3.5	3.5
4198	0.0	0.0	1.7	3.4	1.1	1.1	1	0.00	0.0	0.0
-4199	0.0	0.0	2.3	3.5	NA	NA	1	0.00	0.0	0.0
4200	0.0	0.0	3.8	2.0	1.2	1.2	1	0.00	0.0	0.0
4201	0.0	0.0	3.5	1.5	1.2	1.2	1	0.00	0.0	0.0
4202	0.0	0.0	2.1	3.9	1.0	1.0	1	0.00	0.0	0.0
4206	NA	NA	1.4	1.0	NM	NM	PP	PP	3.2	3.2
-4207	0.0	0.0	111.0	111.0	NA	NA	1	0.00	0.0	0.0
4208	NA	NA	1.5	1.5	NA	NA	PP	PP	4.0	4.0
-4209	0.0	0.0	1.5	1.4	1.3	1.3	1	0.00	0.0	0.0

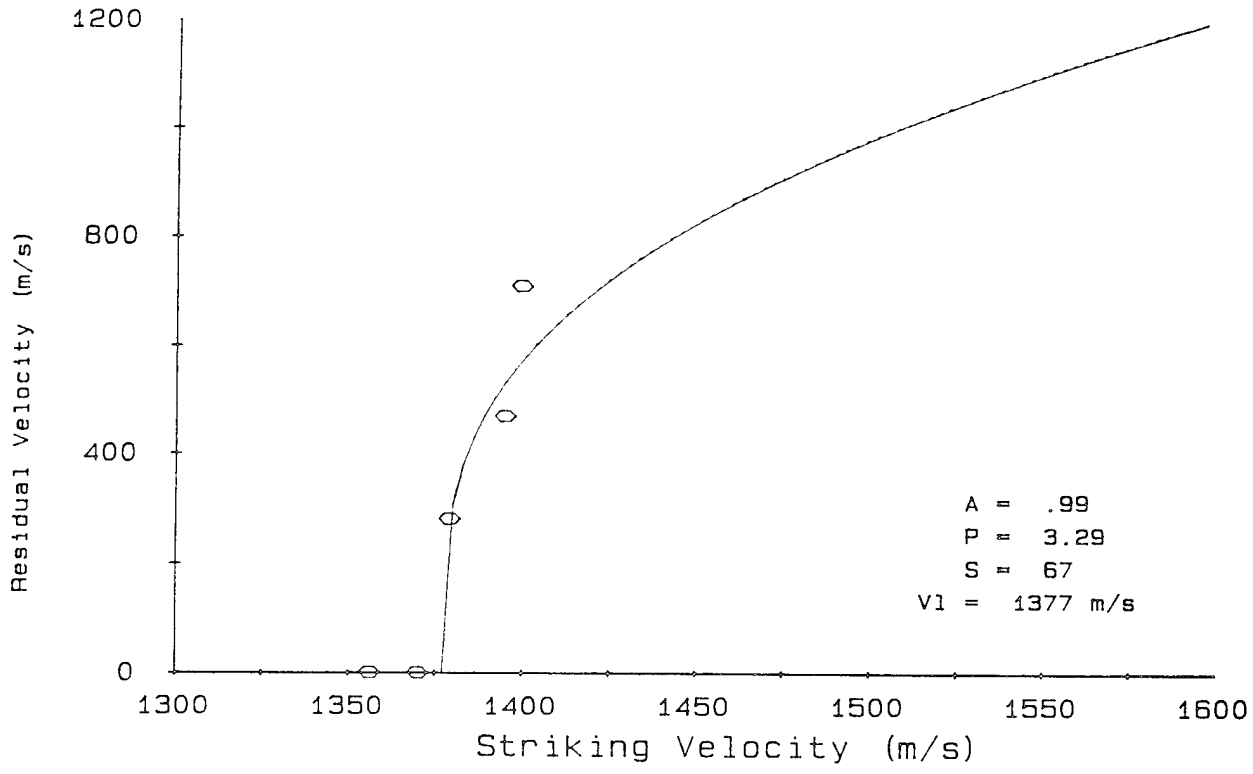

Figure B-3. Vs-Vr curve for penetrators oriented at 90° to rolling direction vs. 3-in RHA at 0°.

Table B-8. Individual Shot Data for Penetrators Oriented at 90° to Rolling Direction vs. Semi-Infinite RHA

Series Fired 5 - 1991
L/D = 15 Density is 17.2

Sh.#	Gamma (deg)	Vs (m/s)	Ms (g)	K.E. (J)	Area (scm)	M/A (g/scm)	KE/A (J/scm)	Norm P/L	Norm Pene. (mm)
4177	1.00	1503	64.98	73395	0.369	176	198693	0.82	84.5

Sh.#	Rise (cm)	Vol base (cc)	Vol total (cc)	KE/Vt (J/cc)	KE/Vb (J/cc)	plV^2 *10^6	Dt/Dp	Area hole (scm)	M/A hole (g/scm)
4177	0.51	8.35	11.02	6660	8790	400	1.60	0.95	68.38
	BHN= 255								

INTENTIONALLY LEFT BLANK.

NO. OF COPIES	ORGANIZATION
2	ADMINISTRATOR DEFENSE TECHNICAL INFO CTR ATTN DTIC DDA CAMERON STATION ALEXANDRIA VA 22304-6145
1	DIRECTOR US ARMY RESEARCH LAB ATTN AMSRL OP SD TA 2800 POWDER MILL RD ADELPHI MD 20783-1145
3	DIRECTOR US ARMY RESEARCH LAB ATTN AMSRL OP SD TL 2800 POWDER MILL RD ADELPHI MD 20783-1145
1	DIRECTOR US ARMY RESEARCH LAB ATTN AMSRL OP SD TP 2800 POWDER MILL RD ADELPHI MD 20783-1145
	ABERDEEN PROVING GROUND
5	DIR USARL ATTN AMSRL OP AP L (305)

NO. OF COPIES	ORGANIZATION
2	COMMANDER USA ARDEC ATTN SMCAR AET B BUSHEY W EBIHARA PCTNY ARSNL NJ 07806-5000
2	COMMANDER USA ARDEC ATTN SMCAR AET M S CYTRON D KAPOOR PCTNY ARSNL NJ 07806-5000
1	COMMANDER USA ARDEC ATTN SMCAR AET M K WILLISON PCTNY ARSNL NJ 07806-5000
1	DIRECTOR US ARMY RESEARCH OFFICE ATTN SLCRO MS A CROWSON PO BOX 12211 RSRCH TRI PK NC 27709-2211
1	DIRECTOR US ARMY RESEARCH OFFICE ATTN SLCRO MS K IYER PO BOX 12211 RSRCH TRI PK NC 27709-2211
1	SOUTHWEST RESEARCH INSTITUTE DEPT OF MECHANICAL SCIENCES ATTN C ANDERSON 8500 CULEBRA RD SAN ANTONIO TX 02912
1	SOUTHWEST RESEARCH INSTITUTE DEPT OF MECHANICAL SCIENCES ATTN J LANKFORD 8500 CULEBRA RD SAN ANTONIO TX 02912
1	SRI INTERNATIONAL ATTN R SHOCKEY 333 RAVENSWOOD AVE MENLO PARK CA 94025
1	DIRECTOR LOS ALAMOS NATL LABORATORY ATTN W HOGAN PO BOX 1663 LOS ALAMOS, NM 87545

NO. OF COPIES	ORGANIZATION
1	DIRECTOR LOS ALAMOS NATL LABORATORY ATTN P DUNN PO BOX 1663 LOS ALAMOS, NM 87545
1	LAWRENCE LIVERMORE NATL LAB ATTN C CLINE PO BOX 808 LIVERMORE CA 94550
1	SANDIA NATL LABORATORIES ATTN V LUK PO BOX 5800 ALBUQUERQUE NM 87185-5800
1	BATTELLE PACIFIC NW LAB ATTN TECH INFO SECTION G DUDDER PO BOX 999 RICHLAND WA 99352
1	BATTELLE PACIFIC NW LAB ATTN TECH INFO SECTION W GURWELL PO BOX 999 RICHLAND WA 99352
1	OAK RIDGE NATL LABORATORY ATTN V SEKKA ONE BETHEL VALLEY RD BLDG 4508 PO BOX 2008 OAK RIDGE TN 37831
1	OAK RIDGE NATL LABORATORY ATTN E OHRINER ONE BETHEL VALLEY RD BLDG 4508 PO BOX 2008 OAK RIDGE TN 37831
	ABERDEEN PROVING GROUND, MD
4	DIR, USARL ATTN: AMSRL-WT-TD, T. FARRAND K. FRANK P. KINGMAN AMSRL-WT-TA, B. BRUCHEY

NO. OF
COPIES ORGANIZATION

ABERDEEN PROVING GROUND, MD (CONT)

11 DIR, USARL
ATTN: AMSRL-WT-TC,
W. LEONARD (3 CPS)
L. MAGNESS
R. SUMMERS
B. WALTERS
E. KENNEDY
W. DE ROSSET
AMSRL-MA-CB,
R. DOWDING
S. CHOU
AMSRL-MA-PD,
T. WEERASOORIYA

INTENTIONALLY LEFT BLANK.

USER EVALUATION SHEET/CHANGE OF ADDRESS

This Laboratory undertakes a continuing effort to improve the quality of the reports it publishes. Your comments/answers to the items/questions below will aid us in our efforts.

1. ARL Report Number ARL-TR-881 Date of Report October 1995

2. Date Report Received _____

3. Does this report satisfy a need? (Comment on purpose, related project, or other area of interest for which the report will be used.) _____

4. Specifically, how is the report being used? (Information source, design data, procedure, source of ideas, etc.) _____

5. Has the information in this report led to any quantitative savings as far as man-hours or dollars saved, operating costs avoided, or efficiencies achieved, etc? If so, please elaborate. _____

6. General Comments. What do you think should be changed to improve future reports? (Indicate changes to organization, technical content, format, etc.) _____

CURRENT ADDRESS

_____
Organization

_____
Name

_____
Street or P.O. Box No.

_____
City, State, Zip Code

7. If indicating a Change of Address or Address Correction, please provide the Current or Correct address above and the Old or Incorrect address below.

OLD ADDRESS

_____
Organization

_____
Name

_____
Street or P.O. Box No.

_____
City, State, Zip Code

(Remove this sheet, fold as indicated, tape closed, and mail.)
(DO NOT STAPLE)

DEPARTMENT OF THE ARMY

OFFICIAL BUSINESS

NO POSTAGE
NECESSARY
IF MAILED
IN THE
UNITED STATES

BUSINESS REPLY MAIL
FIRST CLASS PERMIT NO 0001,APG,MD

POSTAGE WILL BE PAID BY ADDRESSEE

DIRECTOR
U.S. ARMY RESEARCH LABORATORY
ATTN: AMSRL-WT-TC
ABERDEEN PROVING GROUND, MD 21005-5066